



1 Particle size distribution and new particle formation under influence of biomass
2 burning at a high altitude background site of Mt. Yulong (3410m) in China

3

4 Dongjie Shang¹, Min Hu^{1,2*}, Jing Zheng¹, Yanhong Qin¹, Zhuofei Du¹, Mengren Li¹,
5 Jingyao Fang¹, Jianfei Peng¹, Yusheng Wu¹, Sihua Lu¹, Song Guo^{1*}

6 ¹State Key Joint Laboratory of Environmental Simulation and Pollution Control,
7 College of Environmental Sciences and Engineering, Peking University, Beijing,
8 100871, China

9 ²Beijing Innovation Center for Engineering Sciences and Advanced Technology,
10 Peking University, 100871, Beijing, China

11

12 * Corresponding author: E-mail address: minhu@pku.edu.cn, guosong@pku.edu.cn

13 **Abstract**

14 Biomass burning (BB) activities have a great impact on particle number size
15 distribution (PNSD) in upper troposphere of Tibet-Plateau, which could affect
16 regional and global climate. The intensive campaign for the measurement of PNSD,
17 gaseous pollutants and meteorological parameters was conducted at Mt. Yulong, a
18 high-altitude site (3410 m a. s. l.) in the southeast of Tibet Plateau during the
19 pre-monsoon season (22 March to 15 April), when the intensive BB activities in South
20 Asia were observed by fire maps. Long-range transport of BB pollutants could
21 increase the accumulation mode particles in background atmosphere of Mt. Yulong.
22 As a consequence, cloud condensation nuclei (CCN) concentration was found to be
23 2-8 times higher during BB periods than that during clean period. Apart from BB,
24 variation of planet boundary layer (PBL) and new particle formation were other
25 factors that influenced PNSD. However, only 3 NPF events (with a frequency of 14 %)
26 were observed at Mt. Yulong. Occurrence of NPF events during clean episode
27 corresponded with elevated PBL or transported BB pollutants. Due to lack of
28 condensable vapors including sulfuric acid and organic compounds, the newly formed
29 particles were not able to grow to CCN size. Our study emphasized the influences of
30 BB on aerosol and CCN concentration in atmosphere of Tibet Plateau. These results



31 can improve our understanding of the variation of particle concentration in upper
32 troposphere, and provide information for regional and global climate models.

33 Key words: Tibet-Plateau, particle number size distribution, biomass burning,
34 CCN, new particle formation

35 1. Introduction

36 The aerosol particles can influence the radiation of the planet surface through
37 scattering the sunlight, and cloud albedo by serving as cloud condensation nuclei
38 (CCN) (IPCC, 2013). The cloud albedo effect of aerosols provides the biggest
39 uncertainties in global climate models (IPCC, 2013), and depends strongly on number
40 concentration and size of particles. Numerous studies concentrated on monitoring
41 particle number size distribution (PNSD) within the planet boundary layer (PBL),
42 where anthropogenic sources have strong impacts (Peng et al., 2014). While the
43 particles in pristine free troposphere (FT) were rarely studied. Particles in FT mainly
44 originated from lifting of emission within PBL by convective, frontal, and orographic
45 lifting (Okamoto and Tanimoto, 2016), or atmospheric nucleation. Those particles
46 have longer lifetime and could be transported in a longer distance, during which they
47 could exchange with PBL (Shen et al., 2016; D'Andrea et al., 2016). Hence, studies on
48 FT are important because : 1) CCN in FT could influence cloud albedo more directly
49 compared to surface CCN; 2) FT served as a route of long-range transport of
50 pollutants. Aircraft study is a direct way to measure the FT particles, but it is costly
51 and can only provide data within short periods. Therefore, measurement at high
52 mountain sites is one common method to study the FT particles and analyze the
53 influences of pollution transport on FT (Shen et al., 2016).

54 Particles originated from BB in South Asia could have impacts on vast
55 atmosphere of Tibet Plateau by transport in FT. As the highest plateau in the world,
56 Tibet Plateau has very few anthropogenic sources, and could be taken as the continent
57 background. However, recent studies revealed that the smoke plume in South Asia
58 could ascend to FT, and transport to Himalayas and the mountain valley of Tibet
59 Plateau during pre-monsoon season (Cong et al., 2015; Lüthi et al., 2015; Bukowiecki
60 et al., 2016). During pre-monsoon season, the enhanced convection and steep pressure



61 gradient across the Himalaya-Gangetic region could rise the BB particles to higher
62 altitude (Gautam et al., 2009; Adak, 2014). The particles could be transported by dry
63 westerly, and have impacts on aerosols in Tibet Plateau region (Bonasoni et al.,
64 2010; Chen et al., 2014). Former studies verify South Asian BB's influence in Tibet
65 Plateau by chemical analysis of K^+ , levoglucosan, etc. However, there was limited
66 information of variation of PNSD under influence of BB. Also, there were limited
67 studies concerning the contribution of BB to CCN in Tibet Plateau.

68 Except primary emissions, new particle formation (NPF) is another important
69 source of particles in FT, but with limited measurement. According to model results,
70 nucleation in FT contribute to 35 % of the CCN globally (Merikanto et al., 2009).
71 Considering the level of pre-existing particles in FT is relatively low, it should
72 provide a good condition for nucleation of the nanoparticles. As a result, NPF has
73 been observed to happen frequently in FT, including Mt. Tai (1500m a.s.l.) (Shen et
74 al., 2016), Mediterranean Sea (1000m-300m a.s.l.) (Rose et al., 2015), Mt. Puy de
75 Dôme (1465 m a.s.l.), Mt. Izana (2367m a.s.l.) (Rodríguez et al., 2009; García et al.,
76 2014), Colorado Rocky Mountains (2900m a.s.l.) (Boy et al., 2008), etc. While NPF
77 events happened less frequently at Indian foothill Himalayas (2080m) (Neitola et al.,
78 2011). Studies at mountain sites considered that the frequency of NPF corresponded
79 to the rise of PBL height, which could raise the concentration of anthropogenic SO_2 ,
80 NH_3 and other nucleation precursors. Mechanisms of formation and the growth of
81 nanoparticles in FT remain ambiguous (Bianchi et al., 2016), thus comprehensive
82 measurements of PNSD as well as trace gases at high-mountain sites are necessary to
83 provide information around this topic.

84 This study aimed to: 1) investigate the influence of BB from South Asia on
85 PNSD and CCN concentration at South east of Tibet Plateau; 2) characterize the NPF
86 at high-mountain sites. For purposes of these, a comprehensive measurement was
87 conducted at a background site in Mt. Yulong (3140 m a.s.l.), during the pre-monsoon
88 season.

89 **2. Experiments and data analysis**



90 2.1 Monitoring site

91 An intensive field campaign was conducted during 22 March to 15 April, at a
92 high mountains site of Mt. Yulong (27.2N, 100.2E) in Southwest China and Southeast
93 corner of Tibet Plateau, with an altitude of 3140 m a. s. l. This site is one of national
94 regional background sites coordinated by the Chinese Environmental Monitoring
95 Center (CEMC), which is a remote site on the transport route of South Asian
96 pollutants during pre-monsoon season. At the foot of the Mt. Yulong, 36 km to the
97 south of the site is the famous Lijiang Old Town, a populated tourist place. More
98 details of the monitoring site can be found in another paper (Zheng et al., 2017).

99 2.2 Instrumentation

100 PNSD was measured with a time resolution of 5 min, by two set of scanning
101 mobility particle sizer (SMPS, TSI Inc., St. Paul, MN, USA) and an aerodynamic
102 particle sizer (APS, TSI model 3321, TSI Inc., St. Paul, MN, USA). The first set of
103 SMPS consisted of a short differential mobility analyzer (DMA, Model 3085) and an
104 ultra-condensing particle counter (UCPC, Model 3776, flowrate 1.5 L/min) was used
105 to measure the 3-60 nm particles. Another SMPS with long DMA (Model 3081) and
106 normal CPC (Model 3022, flow rate 0.3 L/min) was used for measuring 60-700 nm
107 particles. A silicon diffusion tube was placed before the SMPS, controlling the relative
108 humidity of sampling air under 35 %. Diffusion loss and multiple charging calibration
109 of the particles was done for SMPS data. APS with flow rate of 1 L/min was used for
110 measuring 0.5-10 μm particles. The result of APS was modified to stokes diameter
111 assuming the particle density to be 1.7 $\mu\text{g}/\text{m}^3$ before combining with SMPS data. A
112 bypass flow was added before the inlet cutoff, to meet the working flow rate of the
113 PM_{10} cyclone (16.7 L/min).

114 To investigate the BB influences in aerosols, a high-resolution time-of-flight
115 aerosol mass spectrometer (HR-TOF-AMS) was deployed to measure the chemical
116 composition of aerosols. Through this instrument, we can obtain the concentration of
117 nitrate, sulfate, ammonium, chloride and high-resolution mass spectrum of organics,



118 especially the fragments of BB organic markers. Black carbon (BC) is another
119 important marker for combustion sources. In this study, BC was measured with an
120 aethalometer (Magee Scientific, USA, type AE31), by collecting aerosol particles on a
121 filter stripe, and analyzing the transmission of the lights with seven wave length, from
122 370 to 950 nm. BC concentration was calculated as a multiple of the light absorption
123 coefficient at 880nm, with the default mass attenuation cross sections of $16.6 \text{ m}^2 \text{ g}^{-1}$
124 (Fröhlich et al., 2015). To get the concentration of organic tracers of the new particle
125 formation, an online-gas chromatography coupled with mass spectrometer and flame
126 ionization detectors (GC-MS/FID) was used to measure the non-methane
127 hydrocarbons (NMHCs), including benzene, toluene, monoterpene, etc.
128 Meteorological parameters, $\text{PM}_{2.5}$ and trace gases were also measured by online
129 instruments during the campaign (Table S1).

130

131 2.3 Data processing

132 2.3.1 Backward trajectory analysis

133 The 48h backward trajectories of the air mass were computed at 4000 m a.s.l.
134 (600 m above the ground of the Mt. Yulong site) by the Weather Research and
135 Forecasting (WRF) model (version 3.61) to identify the impacts from South Asia. The
136 fire spots were obtained from the satellite map from Moderate Resolution Imaging
137 Spectroradiometer (MODIS) (<https://firms.modaps.eosdis.nasa.gov/firemap/>). In order
138 to characterize the air mass origin during the NPF events, the 48h backward
139 trajectories at 600 m above the ground were calculated by NOAA HYSPLIT 4
140 (Hybrid Single-Particle Lagrangian Integrated Trajectory) model (Draxier and Hess,
141 1998).

142 2.3.2 Parameterization of NPF

143 The data of each PNSD during NPF was fitted as the sum of three or two mode
144 lognormal distribution (Hussein et al., 2005), including the geometric mean diameter



145 D_m , geometric standard deviation σ_m and total number concentration of each mode.
 146 During the NPF events, the growth rate (GR) was calculated as the variation of the
 147 mean diameter D_m of newly formed mode in unit interval:

$$148 \quad \text{GR} = \frac{\Delta D_m}{\Delta t} \quad (1)$$

149 Formation rate was calculated for nucleation fraction of the particles (3-25 nm), with
 150 the formula:

$$151 \quad J_{3-25} = \frac{dN_{3-25}}{dt} + N_{3-25} \cdot \text{Coag}S_8 + F_{growth} \quad (2)$$

152 in this formula, N_{3-25} is number concentration of particles within size range of 3-25
 153 nm, $\text{Coag}S_8$ is the coagulation rate of particles with diameter of 8 nm, which is the
 154 geometric mean of 3-25 nm. The coagulation rate was calculated as:

$$155 \quad \text{Coag}S(D_p) = \int K(D_p, D'_p) n(D'_p) dD'_p \quad (3)$$

156 in which $n(D'_p)$ is number concentration of particles with size of D'_p ,
 157 $K(D_p, D'_p)$ is the coagulation coefficient between D_p and D'_p particles. During
 158 nucleation events, there were negligible particles that grew beyond 25 nm, so the last
 159 term in formula of was not included (Dal Maso et al., 2005). To quantify the
 160 limitation of NPF from pre-existing particles, the condensation sink was calculated as:

$$161 \quad \text{CS} = 2\pi D \sum_i \beta \cdot D_i \cdot N_i \quad (4)$$

162 where D is the diffusion coefficient of the condensational vapor, e.g. sulfuric acid, β
 163 the transitional regime correction factor, D_i and N_i are the diameter and number
 164 concentration of particles in class i . In calculation described above, all diameters were
 165 dry diameter directly measured from SMPS, so the coagulation and condensation sink
 166 could be underestimated.

167 Sulfuric acid was thought to be the most important precursor of NPF events
 168 (Sipilä et al., 2010), and could contribute to particle growth by condensation (Yue et
 169 al., 2010; Zhang et al., 2012). In this study, the content of H_2SO_4 was calculated by a
 170 pseudo-steady state method (Kulmala et al., 2001):

$$171 \quad [\text{H}_2\text{SO}_4] = k \cdot [\text{OH}][\text{SO}_2] / \text{CS} \quad (5)$$

172 in which $[\text{OH}]$ and $[\text{SO}_2]$ are number concentration of OH radicals and SO_2 , value of



173 k is $10^{-12} \text{ cm}^3\text{s}^{-1}$. $[\text{OH}]$ was estimated by:

$$174 \quad [\text{OH}] = a(I_0^{1D})^\alpha (J_{\text{NO}_2})^\beta \frac{b[\text{NO}_2]+1}{c[\text{NO}_2]^2+d[\text{NO}_2]+1} \quad (6)$$

175 in which $\alpha=0.83$, $\beta=0.19$, $a=4.1 \times 10^9$, $b=140$, $c=0.41$, $d=1.7$ (Ehhalt and Rohrer,
 176 2000). Contribution of sulfuric acid condensation to particle growth was calculated by
 177 Yue et al.'s (2010) method.

178 2.3.3 Calculation of CCN concentration

179 In order to evaluate the variation of indirect climate effects of the particles at Mt.
 180 Yulong, CCN number concentration was estimated from data of PNSD and particle
 181 chemical composition. Firstly, the SNA (sulfate, nitrate, ammonium) was ion-coupled
 182 to get exact chemical compounds of the inorganic salts in particles. NH_4NO_3 , H_2SO_4 ,
 183 NH_4HSO_4 and $(\text{NH}_4)_2\text{SO}_4$ were calculated following the formula:

$$184 \quad n_{\text{NH}_4\text{NO}_3} = n_{\text{NO}_3^-},$$

$$185 \quad n_{\text{H}_2\text{SO}_4} = \max(0, n_{\text{SO}_4^{2-}} - n_{\text{NH}_4^+} + n_{\text{NO}_3^-}),$$

$$186 \quad n_{\text{NH}_4\text{HSO}_4} = \min(2n_{\text{SO}_4^{2-}} - n_{\text{NH}_4^+} + n_{\text{NO}_3^-}, n_{\text{NH}_4^+} - n_{\text{NO}_3^-}),$$

$$187 \quad n_{(\text{NH}_4)_2\text{SO}_4} = \max(n_{\text{NH}_4^+} - n_{\text{NO}_3^-} - n_{\text{SO}_4^{2-}}, 0),$$

188 where n is the mole number of the specific compounds (Gysel et al., 2007). Based on
 189 κ -Köhler theory and Zdanovskii–Stokes–Robinson (ZSR) mixing rule, the
 190 hygroscopic parameter of mixed particles can be calculated as (Petters and
 191 Kreidenweis, 2007):

$$192 \quad \kappa = \sum_1^n \varepsilon_m \kappa_m$$

193 where ε_m is the volume fraction of the composition m in particles, and κ_m is the
 194 hygroscopic parameter of pure composition m . In this research, we consider
 195 secondary inorganic ions, organics and BC as majority composition of particles, and
 196 put them into the ZSR mixing formula. The correlated parameters of the compounds
 197 we used are in table 1.

198 **Table 1. Densities and hygroscopic parameters of the compounds used in CCN**
 199 **calculation**



Species	NH ₄ NO ₃	NH ₄ HSO ₄	(NH ₄) ₂ SO ₄	H ₂ SO ₄	Organics	BC
ρ (kg m ⁻³)	1720	1780	1769	1830	1400	1700
κ	0.67	0.61	0.61	0.91	0.1	0

200

201 Based on κ-Köhler theory, the relationship between κ and D_c under certain
202 supersaturation (S_c) is:

203
$$\kappa = \frac{4A^3}{27D_c^3 \ln^2 S_c}, \quad A = \frac{4\sigma_{s/a} M_w}{RT\rho_w}$$

204 in which σ_{s/a} is the surface tension of water, M_w and ρ_w is the molecular weight and
205 density of water respectively, R is 8.317 J • mol⁻¹ • K⁻¹, T is the ambient temperature.

206 With the κ of the particles, the critical diameter D_c of the CCN activation can be
207 achieved with this formula. Then the number concentration of CCN can be calculated
208 as number concentration of particles larger than D_c.

209 3. Results and discussion

210 3.1 Particle number size distribution

211 3.1.1 Particle and meteorology parameters

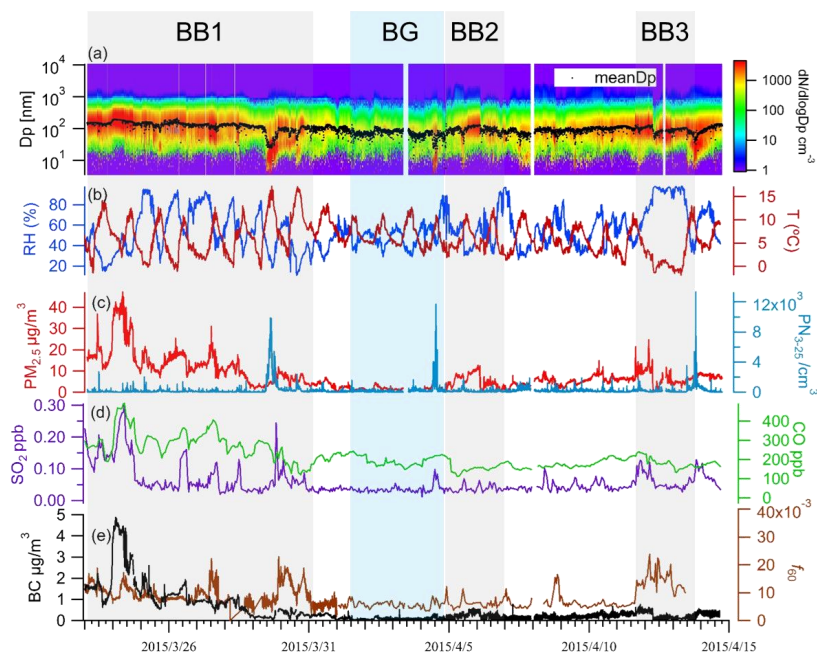
212 Fig.1 shows the time series of PNSD and correlating meteorological parameters.
213 Temperature and relative humidity was 6.1±3.5 °C and 54.9±19.7 %, respectively
214 (Fig.1b). Southeast wind was dominant during the campaign, followed by South wind
215 and Southwest wind. Average wind speed was 2.9±1.8 m/s (Fig S1). Most of the
216 monitoring days were sunny, in favor of nucleation process, while short time rainfall
217 occurred on 24, 26 March and 4, 6, 7, 8, 10, 11 April. During April 12, there was a
218 heavy snow with the RH more than 90 %.

219 As a background high altitude site in TP, Mt. Yulong site revealed the feature of
220 low particle concentration and strong oxidation capacity. On average PM_{2.5} was
221 10.51±9.16 μg/m³, similar with the result on Northeast slope of Tibet Plateau (Xu et
222 al., 2014). This result was only 1/10-1/3 of that in the atmosphere of urban and rural
223 regions in China, indicating a background situation in Southwest China (Zheng et al.,



224 2016). However, the $PM_{2.5}$ at Yulong background site during the monsoon season was
225 around 3 times as that at a Qilian Shan Station in Northeast of Tibet Plateau (Xu et al.,
226 2015) and at Jungfraujoch, Switzerland (Bukowiecki et al., 2016), with similar
227 altitude, indicating relatively stronger anthropogenic influence in Southeast Tibet
228 Plateau. During 22 to 30 March, 4 to 5 April and 11 to 12 April, particle mass
229 concentration exceeded $10 \mu\text{g}/\text{m}^3$, building up a pollution episode.

230 During the measurement, ozone level was 50.1 ± 7.0 ppbv, similar with the results
231 at high mountain sites in Europe (Cristofanelli et al., 2016; Okamoto and Tanimoto,
232 2016), higher than the results in Beijing during spring. The concentration of NO_x and
233 NO was 0.94 ± 0.62 ppbv and 0.07 ± 0.05 ppbv, respectively. SO_2 concentration was
234 0.06 ± 0.05 ppbv, around the detection limit, showing no strong primary pollution. CO
235 concentration was 0.22 ± 0.07 ppmv, and showed higher level during the start of the
236 campaign (24 to 30 March), which could be resulted from the influence of BB (Fig
237 1d).



238
239 **Figure 1. Time series of (a) particle number size distribution and geometric mean**
240 **diameter, (b) ambient temperature, relative humidity, (c) $PM_{2.5}$ mass**



241 **concentration, number concentration of nucleation mode (3-25 nm) particles**
242 **(PN₃₋₂₅), (d) SO₂ and CO concentration, (e) black carbon concentration, fraction**
243 **of f₆₀ (organic fragment ions with m/z=60) during the monitoring campaign.**
244 **Periods influenced by biomass burning (BB1, BB2, BB3) were marked by grey**
245 **shades, period representing background condition (BG) was marked by blue**
246 **shade.**

247 Although particles we measured in this study had larger size range than most of
248 other studies, the results can still be comparable, considering that Aitken and
249 accumulation mode particles, which all measurements included, constitute most of the
250 particle number concentration (PN). Table 2 showed particle number concentrations in
251 atmosphere at Mt. Yulong and other high altitude stations. Total number concentration
252 of PM₁₀ was $1600 \pm 1290 \text{ cm}^{-3}$ during monsoon season of Mt. Yulong, slightly lower
253 than those measured at other sites around Tibet Plateau, e.g. Waliguan and
254 Mukteshwar, and Mt. Huang. However, this result is several times higher than those
255 of areas with scarce emission sources, e.g. Alps and Antarctica. On the other hand, PN
256 didn't show clear trend as the altitude increases, which means the regional emission
257 and transport had larger impact on aerosols in upper troposphere, rather than the
258 vertical distribution. We define N_{3-25} , N_{25-100} , $N_{100-1000}$, N_{1000+} as number
259 concentrations of particles with diameters of 3-25 nm, 25-100 nm, 100-1000 nm and
260 1-10 μm , respectively. There were bursts of N_{3-25} on midday of 29 March, 4 April, 13
261 April, with the peak value at 9900 cm^{-3} , 11700 cm^{-3} and 5400 cm^{-3} , respectively
262 (Fig.1c). During those periods, the geometric mean diameter of the particles was
263 lower than 25 nm. Those events could be resulted from local or regional new particle
264 formation, which would be discussed later.

265

266

267

268

269

270



271 **Table 2. Particle number concentration of high altitude sites around the world, in**
 272 **comparison with this study**

Location	Altitude [m]	Date	Size range [nm]	PN [cm ⁻³]	Reference
Sierra Nevada Mountains, US	1315	May-Nov 2002	10-400	4300	(Lunden et al., 2006)
Mt. Tai, China	1534	July 2010-Feb 2012	3-2500	11800±6200	(Shen et al., 2016)
Mt. Huang, China	1840	April-Aug 2008	10-10000	2350	(Zhang et al., 2016)
Mukteshwar, India	2180	Nov 2005-Nov 2008	10-800	2730	(Komppula et al., 2009)
Izana Observatory, Spain	2367	Nov 2006-Dec 2007	3-660	480-4600	(Rodríguez et al., 2009)
Mt. Norikura, Japan	2770	Sep 2001, July-Sep 2002	9-300	260-1600	(Nishita et al., 2008)
University of Colorado Mountain Research Station, US	2900	July 2006	3-800	2881-19947	(Boy et al., 2008)
Dome C, Antarctica	3200	Spring, 2008-2009	10-600	17.9-457	(Järvinen et al., 2013)
Storm Peak Laboratory, US	3210	Mar 2012	10-10000	3100	(Yu and Hallar, 2014)
Jungfrauoch, Switzerland	3580	1995-2015	10-10000	757	(Bukowiecki et al., 2016)
Wangliguan, China	3816	Sep 2005-May 2007	12-570	2030	(Kivekäs et al., 2009)
Mt. Yulong, China	3410	May-April 2015	3-10000	1600±1290	This Study

273

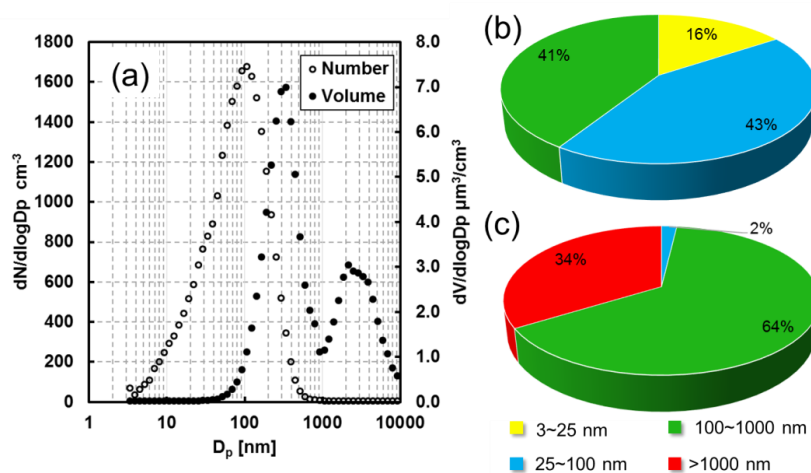
274 3.1.2 Analysis of PNSD and PVSD

275 Average of PNSD during the measurement is showed in Fig.2a. In this study, we
 276 sorted the particles by their sizes (Dal Maso et al., 2005). N_{25-100} correlates to primary
 277 emission, and $PN_{100-1000}$ has stronger connection with secondary formation (Wu et al.,
 278 2008). The diameter with highest particle number concentration (D_{p-max}) was 107 nm.
 279 Number concentration ($dN/d\log D_p$) was larger than 1000 cm^{-3} between 40-200 nm,
 280 which was the adjacent area of N_{25-100} and $N_{100-1000}$. This indicates that both primary
 281 emission sources and secondary formation process had influences at Mt. Yulong site.



282 N_{3-25} , N_{25-100} , $N_{100-1000}$ were 244 cm^{-3} , 676 cm^{-3} and 638 cm^{-3} , constituting 16 %, 43 %
283 and 41 % of total concentration, respectively.

284 Different from PNSD, particle volume (PV) exhibited a bimodal distribution (Fig
285 2a). The first peak had an extreme value at 340 nm, representing the contribution of
286 primary emission and aging processes. This mass peak constituted 66 % of total PV,
287 including PV_{25-100} (2 %) and $PV_{100-1000}$ (64 %). 3-25 nm particles had negligible
288 influence on PV. Another mode in PV size distribution is within range of $1\mu\text{m}$ - $10\mu\text{m}$,
289 with the $D_{p\text{-max}}$ at $2.2 \mu\text{m}$. This mode could be attributed to the suspended soil.
290 Volume of 1- $10\mu\text{m}$ particles constituted 34 % of total PV, similar with Qilian Shan
291 station (38 %) at Northeast Tibet Plateau (Xu et al., 2015), but higher than that urban
292 Beijing (25 %) (Wu et al., 2008), due to the much less emission sources and stronger
293 wind at Mt. Yulong.

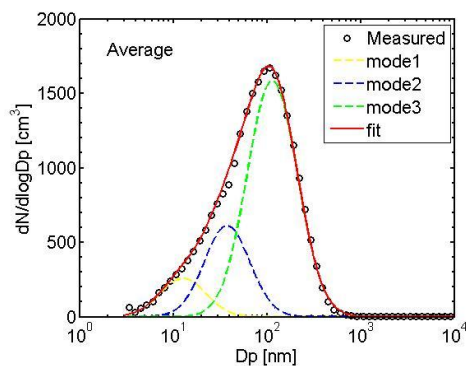


294
295 **Figure 2. Particle size distribution in atmosphere at Mt. Yulong. (a) Mean size**
296 **distribution of particle number (hollow circle) and volume (filled circle)**
297 **concentration; Contribution of different fractions to total particle (b) number**
298 **concentration and (c) volume concentration. Different colors represent different**
299 **size ranges: yellow (3-25 nm), blue (25-100 nm), green (100-1000 nm), red (1-10**
300 **μm).**

301



302 To better characterize the contribution from different process, the mean PNSD
303 was fitted to three lognormal modes (Fig. 3, Table 3). We define the three fitted modes
304 as nucleation mode, Aitken mode and accumulation mode, based on their geometric
305 mean diameters, which were within 3-25 nm, 25-100 nm and 100-1000 nm,
306 respectively. Nucleation mode can be derived from nucleation process. Nucleation
307 mode contributed 15 % to total PN, which was half lower than proportion of
308 nucleation mode particles at Mt. Tai, indicating relatively less impact from nucleation
309 events. Median diameter of Aitken mode and accumulation mode particles are 52 nm
310 and 130 nm. These mean diameters are similar with the results at Jungfrauoch
311 (Bukowiecki et al., 2016) and Beijing (Wu et al., 2008). Accumulation mode particles,
312 correlating with secondary formation (mode_3), contributed 54 % to total PN, which
313 is twice higher than the result in urban Beijing (Wu et al., 2008), and similar with that
314 in pristine atmosphere of Jungfrauoch (Bukowiecki et al., 2016). This result indicates
315 that aerosols arrived at Mt. Yulong were aged during the transport.



316
317 **Figure 3. Lognormal fit (3 modes) of average particle number size distribution**
318 **during the campaign at Mt. Yulong. Black circles mark the measured PNSD,**
319 **colored dash lines represent the PNSD of fitting modes, and red full line marks**
320 **the sum of PNSD of all fitting modes. Mode 1, 2 and 3 were nucleation mode,**
321 **Aitken mode and accumulation mode, respectively.**
322



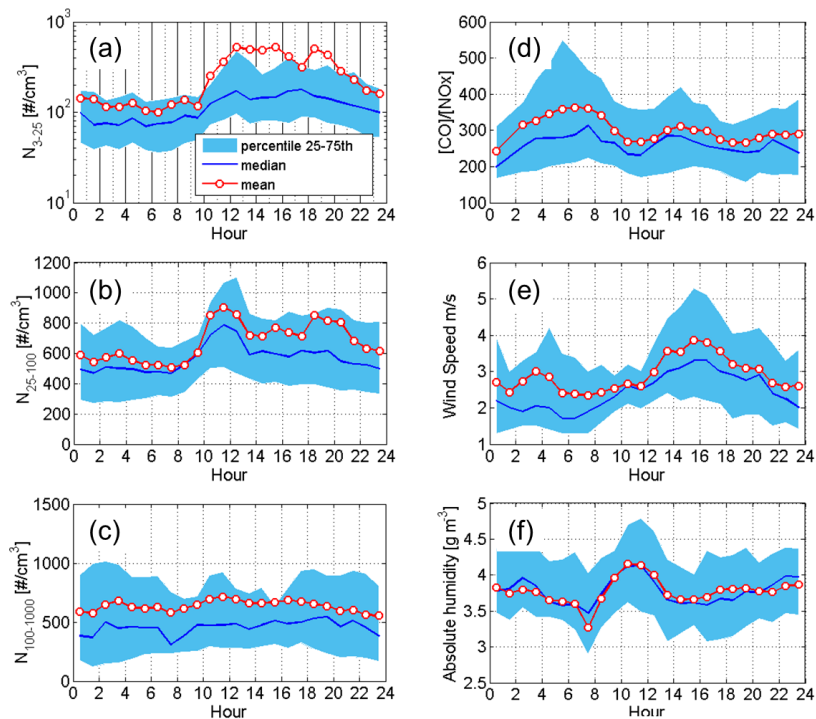
323 3.2 Influence of PBL diurnal variation on PNSD

324 Figure 4 shows the diurnal variation of N_{3-25} , N_{25-100} , $N_{100-1000}$ during the
325 sampling period. The particle number concentration in nucleation fraction and Aitken
326 fraction showed a clear diurnal variation. Mean value of N_{3-25} started to increase at
327 10:00 in the morning, and reached around 500 cm^{-3} at noon due to nucleation events
328 at noon (Fig. 4a). However, the median of N_{3-25} didn't showed similar diurnal
329 variation because of low NPF frequency. On the other hand, both mean and median of
330 N_{25-100} showed a local maximum during 10:00-14:00 (Fig. 4b). NPF events could not
331 cause this variation, since newly formed particles were not able to grow to 25 nm in
332 the morning. So the increased 25-100 nm particles originated from primary sources,
333 e.g. traffic sources and biomass burning. Considering that no anthropogenic emission
334 sources around the site, those primary particles could be transported from other
335 regions. During noon time, as the convection is strongest, N_{25-100} could be raised by
336 the elevated urban PBL during the day, and anthropogenic particle injected during this
337 process (Tröstl et al., 2016b). Adak et al. (2014) also reported that number
338 concentration of PM_{10} increased during day time, corresponding with the up-slope
339 valley wind. In the afternoon, the convection become weaker, and the larger wind
340 speed (Fig. 4e) had stronger scavenging effect on those primary particles, so N_{25-100}
341 decreased at around 14:00.

342 The diurnal change of absolute water content also support that Mt. Yulong site
343 was influenced by elevated PBL during midday. The water concentration was
344 calculated based on temperature and relative humidity, and showed an increase from
345 3.3 g m^{-3} to 4.2 g m^{-3} during 9:00-12:00, and descended back to 3.6 g m^{-3} till 14:00
346 (Fig. 4f). This systematic water content variation indicates that the site was influenced
347 by the PBL during day time. Shen et al (2016) used the increase of water content
348 together with Aitken mode particles, to separate the PBL conditions at Mt. Tai. The
349 value of CO/NO_y and NO_y/NO_x was used in other studies to determine the age of the
350 air masses arriving high altitude sites (Tröstl et al., 2016b; Zellweger et al.,
351 2003; Jaeglé et al., 1998). Because NO_y was not measured in this study, we used



352 CO/NO_x to estimate the age of air mass since contact with primary emission. CO/NO_x
353 was 287±146 at Mt. Yulong, lower than Jungfrauoch (Herrmann et al., 2015), Mt.
354 Cimone (Cristofanelli et al., 2016) and Kansas (Jaeglé et al., 1998), indicating a
355 stronger anthropogenic influence. The diurnal variation of CO/NO_x showed minimum
356 during 9:00-14:00 (Fig. 4d), consistent with the local maximum of water content and
357 N₂₅₋₁₀₀. The diurnal variation of O₃/NO_x exhibited a similar trend as CO/NO_x, with an
358 average of 69.6 during 10:00-14:00, and 83.6 during 1:00-6:00 (Fig. S2). Those
359 evidences indicate that at least during 10:00-14:00, Mt. Yulong site was influenced by
360 elevated PBL. On the other hand, we consider the data during 1:00-6:00 as the
361 condition within FT, when N₂₅₋₁₀₀ and water content were lowest and CO/NO_x were
362 highest. However, N₁₀₀₋₁₀₀₀ didn't show obvious diurnal variation, indicating the
363 elevated PBL didn't inject large amount of 100-1000 nm particles.



364

365 **Figure 4. Diurnal variations of N₃₋₂₅, N₂₅₋₁₀₀, N₁₀₀₋₁₀₀₀, CO/NO_x, wind speed, and**
366 **absolute humidity at Mt. Yulong during monitoring campaign. Red lines with**
367 **circles, blue lines mark the mean and median results, respectively. Light blue**



368 **area marks the range between 25th, and 75th percentiles of the data.**

369 3.3 Influences of BB on Mt. Yulong

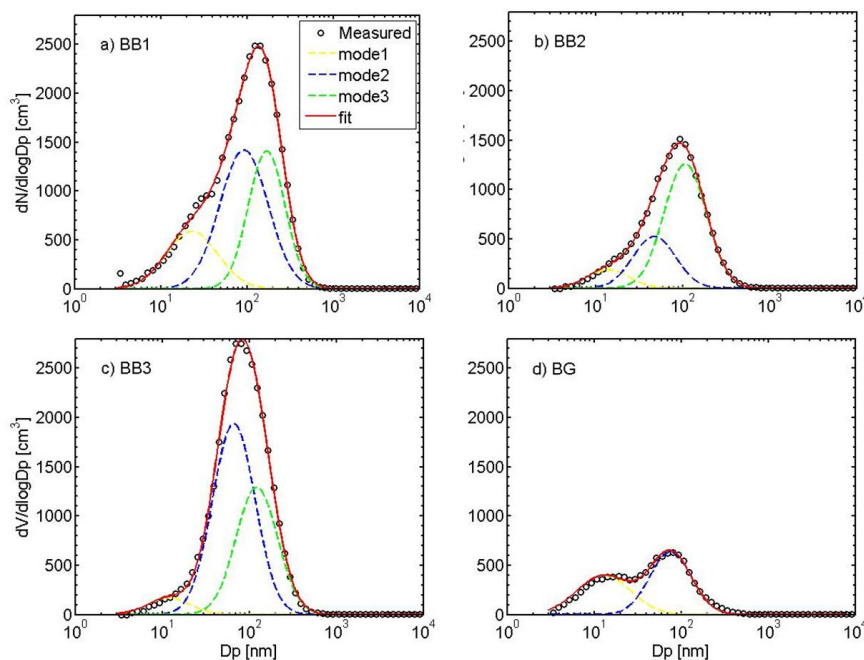
370 3.3.1 Identification of BB episodes

371 Background condition (BG) was picked during 1 to 4 April, when the
372 concentration of BC was 85 ng m^{-3} on average. During this period, the wind was
373 relatively stronger, and fire spots were barely found on the westward path of the air
374 mass (Fig. S3). Based on the background condition, three BB events were identified
375 by the following criteria: 1) BC was more than the background level (85 ng m^{-3}); 2)
376 higher fraction of f_{60} than during BG (0.4 %); 3) fire spots appeared in the source
377 regions of the air masses or surrounding areas of the site.

378 During the first BB event (BB1, 22 to 30 March), dense fire spots were found on
379 the source region in north Burma. BC concentration ($1.2 \text{ } \mu\text{g m}^{-3}$), PV and f_{60} signal
380 showed highest level during BB1. Trajectories of BB2 (5 to 6 April) passed fewer fire
381 spots in South Asia than BB1, and the BC concentration was lower ($0.3 \text{ } \mu\text{g m}^{-3}$). The
382 proportion of f_{60} was highest (1.4 %) during BB3 (11 to 12 April), showing strong
383 BB influence. However, few fire spots were observed on the path of air mass,
384 indicating the BB particles could be derived from domestic heating nearby.



385 3.3.2 Influences of BB on PNSD and CCN



386

387 **Figure 5. Lognormal fit (3 modes) of average PNSD during (a) BB1, (b) BB2, (c)**
388 **BB3, (d) BG at Mt. Yulong site. Black circles mark the measured PNSD, colored**
389 **dash lines represent the PNSD of fitting modes, and red full line marks the sum**
390 **of PNSD of all fitting modes. Mode 1, 2, 3 were nucleation mode, Aitken mode**
391 **and accumulation mode, respectively.**

392 The average PNSDs during BB events and BG condition were plotted in Figure 5,
393 and fitted by 3-mode lognormal distributions. The fitting results are showed in Table 3.
394 For the BG condition, only two modes were obtained (Fig. 5d), including nucleation
395 mode (mode_1, $D_{\text{mean}} = 15$ nm) originated from nucleation events and Aitken mode
396 (mode_2, $D_{\text{mean}} = 79$ nm). Their total number concentration was 669 cm^{-3} , similar
397 with the level at Swiss Jungfraujoeh (Herrmann et al., 2015), exhibiting an Eurasia
398 background character.

399 The averaged PNSD during those BB episodes showed discrepancies, indicating
400 the variant influences of transported and local BB on particles in atmosphere of Mt.



401 Yulong. During the BB2, Aitken mode number concentration was similar with that
402 during BG condition. But an accumulation mode (mode_3, $D_{\text{mean}} = 106$ nm) with
403 higher PN (775 cm^{-3}) appeared (Fig. 5b). This mode with larger size could be the aged
404 particles transported from BB source regions in South Asia. Different from BB2,
405 Aitken mode particles were increased by a factor of 3 and became dominant in PNSD
406 during BB3 the local event (Fig. 5c). The number concentration of this mode was
407 1309 cm^{-3} , 2 times more than accumulation mode particles. The reason could be that
408 the particles during BB3 were freshly emitted from sources nearby the monitoring site.
409 The study of Zheng et al (2017) also showed that during this period, the OOA fraction
410 in organic aerosols was relatively lower, while BBOA fraction was higher, indicating
411 impacts from more local BB sources. The geometric mean diameters of accumulation
412 mode were 169, 106, 130 nm during BB1, BB2, and BB3, smaller than that of aged
413 biomass burning particles at Mt. Bachelor, USA (Laing et al., 2016), indicating the
414 particles at Mt. Yulong were more fresh. Nucleation mode had lower PN during BB2
415 and BB3, since the higher PN of larger particles played as strong coagulation sink of
416 nucleation mode particles. Aitken mode and accumulation mode were comparable
417 during BB1 (Fig. 5a), indicating the fresh aerosols from sources surrounding the site
418 had comparable influence as the transported aged BB aerosols.

419 In a word, the BG condition at Mt. Yulong could represent the background level
420 of particles of TP or even Eurasia. The local and long-range transported BB emissions
421 would increase the level of Aitken mode and accumulation mode particles,
422 respectively.

423

424

425

426

427

428

429

430



431 **Table 3. Fitted parameters of lognormal modes for different period. μ , σ and N**
 432 **represent the mean diameter, standard deviation, and total number**
 433 **concentration of each mode, respectively. “Total” represents the mean result of**
 434 **all data achieved from the campaign.**

Period	μ [nm]			σ [nm]			N [cm ⁻³]		
	mode_1	mode_2	mode_3	mode_1	mode_2	mode_3	mode_1	mode_2	mode_3
Total	16	52	130	1.75	1.75	1.77	221	488	861
BB1	23	92	169	1.94	1.91	1.63	428	1014	744
BB2	16	47	106	1.75	1.75	1.75	117	302	775
BB3	15	70	130	1.75	1.75	1.72	106	1309	628
BG	15	79	-	2.03	1.73	-	301	368	-

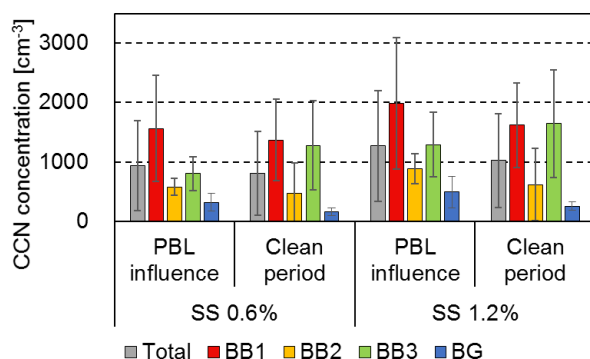
435

436 Concentration of CCN was calculated following method described in section
 437 2.3.3. κ value during the sampling period was 0.12 ± 0.01 , only 1/3 from urban Beijing
 438 (Wu et al., 2016) and a rural site at Thuringia, Germany (Wu et al., 2013), but
 439 consistent with the results in Alberta, Canada (0.11 ± 0.04) during BB events (Latham
 440 et al., 2013). Pierce et al (2012) reported that κ was around 0.1 for >100 nm particles
 441 in a forest mountain valley during biogenic secondary organic aerosols formation and
 442 growth events. Similarly, organic volume fraction was 0.73 in particle at Mt. Yulong,
 443 explaining the low value of κ . As a result, the D_c at SS of 0.6 % and 1.2 % was
 444 72.0 ± 2.2 and 45.4 ± 1.4 nm, respectively. There could be uncertainties for value of κ
 445 and D_c , since here we used a manually set hygroscopicity of organics, which may
 446 varied with oxidation level or other factors (Wu et al., 2016). Considering the
 447 variation range of D_c was small, the CCN concentration was mainly controlled by size
 448 distribution of particle number.

449 BB events raised the CCN level in atmosphere by influencing the PNSD.
 450 Increase of PN was observed during BB events, i.e. 2207 ± 1388 cm⁻³, 1214 ± 638 cm⁻³,
 451 2062 ± 1112 cm⁻³ during BB1, BB2, BB3, respectively. As a consequence, the
 452 increased particles played as CCN in atmosphere of Mt. Yulong, forming a readily
 453 increase of CCN concentration during BB events. Figure 6 showed the mean number
 454 concentration of CCN in periods under PBL influence (10:00-14:00, as discussed in
 455 3.2) and FT condition (1:00-6:00) during BG and BB events. Mean number



456 concentration of CCN under supersaturation of 0.6 % was $936 \pm 754 \text{ cm}^{-3}$ and 807 ± 705
457 cm^{-3} for PBL and FT periods at Mt. Yulong, comparative with boreal forest station in
458 Finland (Cerully et al., 2011). The concentration of CCN in PBL condition during
459 BB1, BB2, BB3 was 5, 2, 2 times as that during BG. Promotions of CCN during BB1,
460 BB2, BB3 were more remarkable for FT, i.e. 9, 3, 8 times as BG (Fig. 6). This result
461 indicates that the BB particles from South Asia could have strong influence on the
462 climate parameter. For the data under supersaturation of 1.2 %, the ratios between
463 CCN concentration of BBs and that of BG were less, i.e. 2-4 times for periods
464 influenced by PBL, and 2-7 times for FT conditions. This is because critical diameters
465 under supersaturation 0.6 % and 1.2 % were around 72 nm and 45 nm, respectively.
466 And PN within 45-72 nm was relatively stable compared to the larger particles,
467 because of the daily input of anthropogenic primary aerosols from urban air masses.



468
469 **Figure 6. Mean number concentration of CCN under supersaturation of 0.6 %**
470 **and 1.2 % during whole monitoring period (labelled as “total”), BB1, BB2, BB3**
471 **events (marked by shadow in Fig. 1). PBL (10:00-14:00) and FT (1:00-6:00)**
472 **conditions were separated.**

473

474 3.4 New particle formation events

475 3.4.1 NPF events at Mt. Yulong under anthropogenic influences

476 Following the method Tröstl et al (2016b) and Yli-Juuti et al (2009) used, we



477 define the three NPF events on 29 March, 4 and 13 April as follows:

478 a) Type A event on 29 March: appearance of newly formed particles (3 nm, the first
479 bin of nano-SMPS) and continuous growth of those particles, reaching the upper
480 limit of nucleation mode (25 nm). This NPF event was within the period of BB1,
481 the air mass arriving at Mt. Yulong was from North part of Burma with slow
482 movement before 28 March, transporting abundant pollutants to this area. During
483 28 March 12:00 to 29 March 6:00, the air mass was from west upper troposphere
484 (Fig S4), cleaning out the pre-existing particles built up by BB events. CS at Mt.
485 Yulong decreased from 0.006 s^{-1} to 0.002 s^{-1} on morning of 29 March. On the
486 other hand, the concentration of SO_2 was stable (around 0.04 ppb) before
487 occurrence of nucleation. The calculated H_2SO_4 increased before nucleation,
488 reaching $5 \times 10^6 \text{ cm}^{-3}$ (Fig. S4). The nucleation rate was $1.43 \text{ cm}^{-3}\text{s}^{-1}$, increasing
489 nucleation mode particles to around 10^4 cm^{-3} . Benefited by the increase of
490 α -pinene (from 0.02 ppb to 0.10 ppb), β -pinene (from 0.03 ppb to 0.20 ppb) and
491 SO_2 in day of 29 March, the formation of secondary aerosol continued, and the
492 newly formed particles grew over 30 nm before night. This process could be from
493 gaseous oxidation and condensation. Particle growth stopped during night of 29
494 March, when the gaseous reaction was inhibited because of absence of sunlight.
495 After sunrise on 30 March, the particle continued growing and reached 40 nm.
496 Concentration of toluene was lower than 0.1 ppb, indicating small contribution
497 from anthropogenic VOCs. The GR was 3.48 nm h^{-1} within size range of 3-25 nm.
498 In a word, under the influence of transported pollutants, nucleation was triggered
499 by the upper clean air mass, which reduced level of pre-existing particles. While
500 growth of particles was favored by the photochemical reaction and condensation
501 process.

502

503 b) Type B event on 4 April: newly formed mode occurred with growing trend, but
504 growth stopped at early stage (<15 nm), and there were temporal low values of
505 N_{3-25} during the event. The event on 4 April was under BG condition, during
506 which concentration of SO_2 was lower (around 0.02 ppb). Started from 2:00 on 4



507 April, the air mass arrived at Mt. Yulong was transported by upslope flow from
508 west lower troposphere. While during 9:00-12:00, the air mass arrived at Mt.
509 Yulong passed Northeast India, where fire spots could be observed on the MODIS
510 map during 2 April. Thus, the gaseous pollutants and particles from anthropogenic
511 sources nearby or from BB sources in Northeast India was transported to this site
512 on morning of 4 April. Concentration of SO₂ and [H₂SO₄] increased to 0.07 ppb
513 and 6×10⁶ cm⁻³ at 11:00, respectively, corresponding to occurrence nucleation (Fig.
514 S5). SO₂ shared similar time series with black carbon, indicating a combustion
515 source. FR and GR were 0.93 cm⁻³ s⁻¹ and 3.2 nm h⁻¹, respectively. N₃₋₂₅ fluctuated
516 during NPF events, showing low values when there were temporary changes in
517 cloud condition (influencing radiation) and wind direction. Concentrations of
518 β-pinene and Toluene were stable and lower than 0.10 ppb and 0.65 ppb
519 respectively throughout the NPF event, which could be the reason of smaller
520 growth rate. At around 14:00, the source region of air mass varied to west upper
521 troposphere, and the stronger wind cleaned out both the nucleated mode particles
522 and gaseous precursors, terminating the NPF event. In summary, type B event
523 under background condition was triggered by the injection of gaseous pollutants
524 from elevated PBL and short term transport of BB pollutants.

525

526 c) Off-site NPF event on 13 April: A narrow Aitken mode band (25-50 nm) was
527 observed from 13 to 14 April. The primary particles should have wider range and
528 larger size. These particles were mostly likely nucleated off-site, and transported
529 to Mt. Yulong site by uplifting air mass. On the afternoon of 13 April, the air mass
530 arrived at Mt. Yulong passed the local ground layer (yellow trajectory in Fig S6).
531 SO₂ increased from 0.06 ppb to 0.13 ppb, and toluene reached highest level at
532 0.098 ppb (Fig. S6), indicating an anthropogenic impact. As a result, particles
533 formed from the ground level were transported to the site and a burst of N₃₋₂₅
534 occurred at around 18:00, with FR at 1.64 cm⁻³ s⁻¹. β-pinene also showed higher
535 value at dawn of 13 April. Those nanoparticles showed a growth trend, with GR at
536 2.99 nm h⁻¹. To summarize, occurrence of nucleation mode particles were off-site



537 nucleated in PBL and transported to this site.

538

539 3.4.2 Limiting factors of NPF events

540 Frequency of NPF was 14 % during our measurement. This NPF frequency is
541 clearly less than polluted atmosphere of North China Plain (40-65 %) in March and
542 April (Wang et al., 2013; Shen et al., 2011), the top of Mt. Huang (38 %) during April
543 (Zhang et al., 2016), and a remote rural site in the Sierra Nevada Mountains (47 %) in
544 spring (Creamean et al., 2011). A common knowledge is that CS is the limiting factor
545 that controls the NPF (Cai et al., 2017). Thus, pre-existing particle levels on event
546 days should be less than non-event days, at high altitude mountain sites (Shen et al.,
547 2016; Guo et al., 2012) as well as urban sites (Wang et al., 2011; Wang et al., 2017).
548 The low NPF frequency was unexpected in clean atmosphere of Mt. Yulong, since the
549 mean CS at Mt. Yulong was 0.0038 s^{-1} . On the other hand, similar low frequency of
550 NPF events were also observed in pristine atmospheres, e.g. 24 % at Antarctic site
551 Neumayer (Weller et al., 2015), 12-17 % at Dome C, Antarctica (Järvinen et al.,
552 2013).

553 During the first five days of the campaign (22 to 27 March), the nucleation
554 events could be prevented by large amount of pre-existing particles acting as big
555 condensation sink. The CS was more than 0.005 s^{-1} , similar with polluted Beijing on
556 days with NPF events (Wu et al., 2007). However, on rest of days when CS was even
557 lower than 0.002 s^{-1} , the NPF events were still scarce. Considering that the content of
558 condensable vapor participated in nucleation is determined by the competition
559 between formation from precursor oxidation and condensation on surface of
560 pre-existing particles (Zhang et al., 2012), the lower NPF frequency at pristine sites
561 could be resulted from lack of precursor, e.g. VOCs and SO_2 from fossil fuel and
562 biomass burning sources.

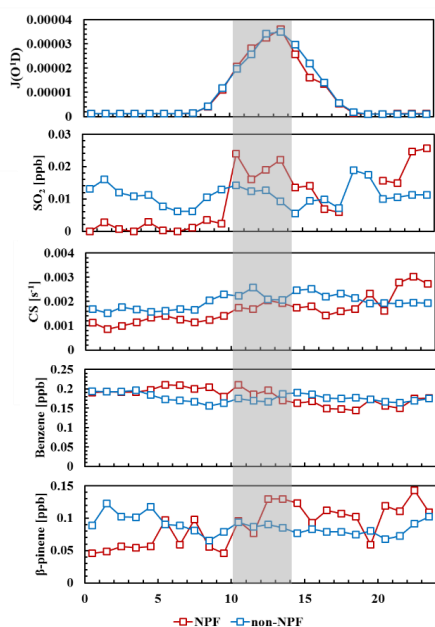
563 To further evaluate the effect of different parameters on NPF, daily variations of
564 SO_2 , CS, $\text{J}(\text{O}^1\text{D})$, Benzene and β -pinene during 28 March to 14 April were calculated
565 and plotted in Figure 7. The results during 10:00-14:00 were picked up as the



566 occurrence time of nucleation, and compared between NPF days and non-event days.
567 As shown in Fig. 7, NPF days and non-NPF days shared same level of $J(O^1D)$, and
568 15 % difference in CS when nucleation happened, indicating small influence of solar
569 radiation and pre-existing particles on NPF.

570 The concentration of SO_2 showed increase on NPF days, 60 % higher than
571 non-event days, indicating the anthropogenic SO_2 as the controlling factor of NPF at
572 Mt. Yulong. Studies at Jungfraujoch (Bianchi et al., 2016; Tröstl et al., 2016b), Izaña
573 (García et al., 2014) and Mukteshwar (Neitola et al., 2011) also reported that the
574 nucleation events in upper troposphere corresponded to increase of anthropogenic gas
575 pollutants by elevated PBL. At Daban Mountain on the North slope of TP, the $PM_{2.5}$
576 level was similar with Mt. Yulong, but NPF could be observed nearly every day. It
577 may be caused by that the SO_2 was around 2 ppb on average, two order of magnitude
578 higher than Mt. Yulong.

579 Organics may also be a driven factor on NPF. The concentration of β -pinene
580 showed higher value (40 %) in the afternoon on NPF days, while there was little
581 difference (9 %) between NPF days and non-event days on anthropogenic benzene.
582 Recent studies considered that apart from sulfuric acid, the highly oxidized
583 multifunctional organics from biogenic VOCs could take part in nucleation as well as
584 growth (Huang et al., 2016; Tröstl et al., 2016a), in free troposphere, the pure organic
585 nucleation without sulfuric acid may even be dominant (Bianchi et al., 2016; Gordon
586 et al., 2016). So the increase of biogenic VOCs could benefit the nucleation and
587 growth of nucleation mode particles at Mt. Yulong.



588

589 **Figure 7. Diurnal variation of $J(O^1D)$, SO_2 , CS, Benzene, β -pinene during days**
590 **with NPF events (labelled as “NPF”, red lines with marks), and without NPF**
591 **events (labelled as “non-NPF”, blue lines with marks). Shadow marks the time**
592 **period during which nucleation occurred.**

593

594 3.4.3 Parameters of NPF events at Mt. Yulong

595 Formation rate, growth rate and condensation sink of NPF events at Mt. Yulong
596 were summarized in Table 4. Compared with other high mountain measurements, this
597 study reported a higher FR, e.g. 3 times as that at Storm peak laboratory (Hallar et al.,
598 2011). But the GR at Mt. Yulong was within average level, indicating different
599 precursors participating in nucleation and growth process. Even though SO_2 was well
600 correlated with nucleation events, the calculated growth rate by condensation of
601 H_2SO_4 can only explain 5 % of the measured GR. This result indicated participation
602 of some other precursors in particle growth, e.g. organics.

603

604



605 **Table 4. Comparisons of NPF parameters (FR, GR, CS) with the other studies.**

Site	Region	Altitude [m]	Size [nm]	FR [cm ⁻³ s ⁻¹]	GR [nm h ⁻¹]	CS [s ⁻¹]	Reference
Mt. Yulong	Asia	3410	3-25	1.33	3.22	0.002	This research
Mukteshwar	Asia	2180	15-20	0.44	2.47	0.015	(Neitola et al., 2011)
Storm peak laboratory	North America	3210	9-334	0.39	7.5	0.001	(Hallar et al., 2011)
Mt. Tai	Asia	1500	3-25	4	6.1	0.02	(Shen et al., 2016)
Izaña	Atlantic Ocean	2400	10-25	0.46	0.43	0.002	(García et al., 2014)
Jungfrauoch	Europe	3580	3.2-15	1.8	4.0	-	(Tröstl et al., 2016b)
Dome C	Antarctica	3200	10-25	0.023	2.5	0.0002	(Järvinen et al., 2013)

606

607 4. Conclusion

608 PNSD, meteorological parameters, trace gases and particle chemical composition
609 were measured at Mt. Yulong site (3410 m a.s.l.) in Southeast corner of Tibet Plateau,
610 during pre-monsoon season (22 March to 15 April) of 2015. PNSD in background
611 atmosphere of Tibet Plateau was characterized. As a background site in Southwest
612 China, the atmosphere of Mt. Yulong exhibited a feature of low particle level and
613 strong oxidation.

614 PBL convection is an influencing factor of PNSD, which caused readable diurnal
615 variation of N_{air} . Diurnal variation of CO/NO_x and absolute humidity showed that the
616 monitoring site was influenced by PBL during 10:00-14:00, and showed typical FT
617 condition during 1:00-6:00.

618 Three different types of BB event periods were identified by content of BC, f_{60} ,
619 air mass backward trajectory and fire spot map. Accumulation mode was dominant in
620 transported BB particles from Myanmar, but less aged compared with other Tibet
621 Plateau sites under influence of BB. Under local biomass burning episode, Aitken
622 mode was dominant in PNSD. The biomass burning from South Asia had strong
623 influence on climate parameters, especially for FT. Concentrations of CCN in FT at
624 Mt. Yulong during BB events were 3-9 times as that during BG period. Due to high
625 fraction of organic compounds, the CCN activity of particles in atmosphere of Mt.
626 Yulong was lower than other high altitude sites and ground level sites.



627 Unexpected low NPF frequency was found in clean atmosphere at Mt. Yulong,
628 due to low concentration of anthropogenic precursor, i.e. SO₂. Occurrence of NPF
629 events were favored by elevated surface emission of SO₂ and transported BB
630 pollutants from South Asia. Off-site NPF event was also observed, during which
631 nanoparticles were formed in PBL and transported to the site. Condensation of
632 sulfuric acid can only explain 5 % of GR in on-site NPF events, indicating other
633 precursors participating in particle growth. NPF can hardly contribute to CCN, since
634 the newly formed particles cannot reach the critical diameter.

635 Our study provided important data in vertical profile of particles at Tibet Plateau.
636 Influences of BB activities in South Asia and local area on PNSD and CCN in
637 atmosphere of Tibet Plateau were highlighted. Different types of NPF in upper
638 troposphere in Southwest China were characterized, and role of SO₂ were analyzed.
639 Results of our study could be used in regional and global climate model, and help
640 building up the knowledge of NPF in upper part of troposphere.

641

642 **Acknowledgement**

643 This study was supported by National Natural Science Foundation of China
644 (91544214, 41421064, 51636003, 21677002), National Key Research and
645 Development Program of China (2016YFC0202000: Task 3), the China Ministry of
646 Environmental Protection Special Funds for Scientific Research on Public Welfare
647 (201309016). We also thank the colleagues in the China National Environmental
648 Monitoring Center and Lijiang Monitoring Station for the support to the field
649 campaign.

650

651 **References**

- 652 Adak, A.: Atmospheric Fine Mode Particulates at Eastern Himalaya, India: Role of Meteorology,
653 Long-Range Transport and Local Anthropogenic Sources, *Aerosol and Air Quality Research*,
654 10.4209/aaqr.2013.03.0090, 2014.
- 655 Bianchi, F., Tröstl, J., Junninen, H., Frege, C., Henne, S., Hoyle, C. R., Molteni, U., Herrmann, E.,
656 Adamov, A., Bukowiecki, N., Chen, X., Duplissy, J., Gysel, M., Hutterli, M., Kangasluoma, J.,
657 Kontkanen, J., Kürten, A., Manninen, H. E., M ünch, S., Per ä kyl ä O., Pet ä ä T., Rondo, L., Williamson,
658 C., Weingartner, E., Curtius, J., Worsnop, D. R., Kulmala, M., Dommen, J., and Baltensperger, U.: New



- 659 particle formation in the free troposphere: A question of chemistry and timing, *Science*, 352, 1109,
660 2016.
- 661 Bonasoni, P., Laj, P., Marinoni, A., Sprenger, M., Angelini, F., Arduini, J., Bonafè U., Calzolari, F.,
662 Colombo, T., Decesari, S., Di Biagio, C., di Sarra, A. G., Evangelisti, F., Duchi, R., Facchini, M. C.,
663 Fuzzi, S., Gobbi, G. P., Maione, M., Panday, A., Roccatò, F., Sellegri, K., Venzac, H., Verza, G. P.,
664 Villani, P., Vuillermoz, E., and Cristofanelli, P.: Atmospheric Brown Clouds in the Himalayas: first two
665 years of continuous observations at the Nepal Climate Observatory-Pyramid (5079 m), *Atmos. Chem.*
666 *Phys.*, 10, 7515-7531, [10.5194/acp-10-7515-2010](https://doi.org/10.5194/acp-10-7515-2010), 2010.
- 667 Boy, M., Karl, T., Turnipseed, A., Mauldin, R. L., Kosciuch, E., Greenberg, J., Rathbone, J., Smith, J.,
668 Held, A., Barsanti, K., Wehner, B., Bauer, S., Wiedensohler, A., Bonn, B., Kulmala, M., and Guenther,
669 A.: New particle formation in the Front Range of the Colorado Rocky Mountains, *Atmos. Chem. Phys.*,
670 8, 1577-1590, [10.5194/acp-8-1577-2008](https://doi.org/10.5194/acp-8-1577-2008), 2008.
- 671 Bukowiecki, N., Weingartner, E., Gysel, M., Coen, M. C., Zieger, P., Herrmann, E., Steinbacher, M.,
672 Gäggeler, H. W., and Baltensperger, U.: A Review of More than 20 Years of Aerosol Observation at the
673 High Altitude Research Station Jungfraujoch, Switzerland (3580 m asl), *Aerosol and Air Quality*
674 *Research*, 16, 764-788, [10.4209/aaqr.2015.05.0305](https://doi.org/10.4209/aaqr.2015.05.0305), 2016.
- 675 Cai, R., Yang, D., Fu, Y., Wang, X., Li, X., Ma, Y., Hao, J., Zheng, J., and Jiang, J.: Aerosol Surface
676 Area Concentration: a Governing Factor for New Particle Formation in Beijing, *Atmos. Chem. Phys.*
677 *Discuss.*, 2017, 1-26, [10.5194/acp-2017-467](https://doi.org/10.5194/acp-2017-467), 2017.
- 678 Cerully, K. M., Raatikainen, T., Lance, S., Tkacik, D., Tiitta, P., Petäjä T., Ehn, M., Kulmala, M.,
679 Worsnop, D. R., Laaksonen, A., Smith, J. N., and Nenes, A.: Aerosol hygroscopicity and CCN
680 activation kinetics in a boreal forest environment during the 2007 EUCAARI campaign, *Atmospheric*
681 *Chemistry and Physics*, 11, 12369-12386, [10.5194/acp-11-12369-2011](https://doi.org/10.5194/acp-11-12369-2011), 2011.
- 682 Chen, Y., Cao, J., Zhao, J., Xu, H., Arimoto, R., Wang, G., Han, Y., Shen, Z., and Li, G.: N-alkanes and
683 polycyclic aromatic hydrocarbons in total suspended particulates from the southeastern Tibetan Plateau:
684 concentrations, seasonal variations, and sources, *The Science of the total environment*, 470-471, 9-18,
685 [10.1016/j.scitotenv.2013.09.033](https://doi.org/10.1016/j.scitotenv.2013.09.033), 2014.
- 686 Cong, Z., Kang, S., Kawamura, K., Liu, B., Wan, X., Wang, Z., Gao, S., and Fu, P.: Carbonaceous
687 aerosols on the south edge of the Tibetan Plateau: concentrations, seasonality and sources, *Atmos.*
688 *Chem. Phys.*, 15, 1573-1584, [10.5194/acp-15-1573-2015](https://doi.org/10.5194/acp-15-1573-2015), 2015.
- 689 Creamean, J. M., Ault, A. P., Ten Hoeve, J. E., Jacobson, M. Z., Roberts, G. C., and Prather, K. A.:
690 Measurements of aerosol chemistry during new particle formation events at a remote rural mountain
691 site, *Environmental science & technology*, 45, 8208-8216, [10.1021/es103692f](https://doi.org/10.1021/es103692f), 2011.
- 692 Cristofanelli, P., Landi, T. C., Calzolari, F., Duchi, R., Marinoni, A., Rinaldi, M., and Bonasoni, P.:
693 Summer atmospheric composition over the Mediterranean basin: Investigation on transport processes
694 and pollutant export to the free troposphere by observations at the WMO/GAW Mt. Cimone global
695 station (Italy, 2165 m a.s.l.), *Atmospheric Environment*, 141, 139-152, [10.1016/j.atmosenv.2016.06.048](https://doi.org/10.1016/j.atmosenv.2016.06.048),
696 2016.
- 697 D'Andrea, S. D., Ng, J. Y., Kodros, J. K., Atwood, S. A., Wheeler, M. J., Macdonald, A. M., Leitch, W.
698 R., and Pierce, J. R.: Source attribution of aerosol size distributions and model evaluation using
699 Whistler Mountain measurements and GEOS-Chem-TOMAS simulations, *Atmos. Chem. Phys.*, 16,
700 383-396, [10.5194/acp-16-383-2016](https://doi.org/10.5194/acp-16-383-2016), 2016.
- 701 Dal Maso, M., Kulmala, M., Riipinen, I., Wagner, R., Hussein, T., Aalto, P. P., and Lehtinen, K. E. J.:
702 Formation and growth of fresh atmospheric aerosols: eight years of aerosol size distribution data from



- 703 SMEAR II, Hyytiälä, Finland, *Boreal Environ. Res.*, 10, 323-336, 2005.
- 704 Draxier, R. R., and Hess, G. D.: An overview of the HYSPLIT_4 modelling system for trajectories,
705 dispersion and deposition, *Aust. Meteorol. Mag.*, 47, 295-308, 1998.
- 706 Ehhalt, D. H., and Rohrer, F.: Dependence of the OH concentration on solar UV, *J Geophys Res-Atmos*,
707 105, 3565-3571, 10.1029/1999jd901070, 2000.
- 708 Fröhlich, R., Cubison, M. J., Slowik, J. G., Bukowiecki, N., Canonaco, F., Croteau, P. L., Gysel, M.,
709 Henne, S., Herrmann, E., Jayne, J. T., Steinbacher, M., Worsnop, D. R., Baltensperger, U., and Prévôt,
710 A. S. H.: Fourteen months of on-line measurements of the non-refractory submicron aerosol at the
711 Jungfraujoch (3580 m a.s.l.) – chemical composition, origins and organic aerosol sources, *Atmos.*
712 *Chem. Phys.*, 15, 11373-11398, 10.5194/acp-15-11373-2015, 2015.
- 713 Garc ía, M. I., Rodr íguez, S., Gonz ález, Y., and Garc ía, R. D.: Climatology of new particle formation at
714 Izaña mountain GAW observatory in the subtropical North Atlantic, *Atmos. Chem. Phys.*, 14,
715 3865-3881, 10.5194/acp-14-3865-2014, 2014.
- 716 Gautam, R., Hsu, N. C., Lau, K. M., Tsay, S. C., and Kafatos, M.: Enhanced pre-monsoon warming
717 over the Himalayan-Gangetic region from 1979 to 2007, *Geophysical Research Letters*, 36, n/a-n/a,
718 10.1029/2009gl037641, 2009.
- 719 Gordon, H., Sengupta, K., Rap, A., Duplissy, J., Frege, C., Williamson, C., Heinritzi, M., Simon, M.,
720 Yan, C., Almeida, J., Trostl, J., Nieminen, T., Ortega, I. K., Wagner, R., Dunne, E. M., Adamov, A.,
721 Amorim, A., Bernhammer, A. K., Bianchi, F., Breitenlechner, M., Brilke, S., Chen, X. M., Craven, J. S.,
722 Dias, A., Ehrhart, S., Fischer, L., Flagan, R. C., Franchin, A., Fuchs, C., Guida, R., Hakala, J., Hoyle, C.
723 R., Jokinen, T., Junninen, H., Kangasluoma, J., Kim, J., Kirkby, J., Krapf, M., Kurten, A., Laaksonen,
724 A., Lehtipalo, K., Makhmutov, V., Mathot, S., Molteni, U., Monks, S. A., Onnela, A., Perakyla, O., Piel,
725 F., Petaja, T., Praplanh, A. P., Pringle, K. J., Richards, N. A. D., Rissanen, M. P., Rondo, L., Sarnela, N.,
726 Schobesberger, S., Scott, C. E., Seinfeldo, J. H., Sharma, S., Sipila, M., Steiner, G., Stozhkov, Y.,
727 Stratmann, F., Tome, A., Virtanen, A., Vogel, A. L., Wagner, A. C., Wagner, P. E., Weingartner, E.,
728 Wimmer, D., Winkler, P. M., Ye, P. L., Zhang, X., Hansel, A., Dommen, J., Donahue, N. M., Worsnop,
729 D. R., Baltensperger, U., Kulmala, M., Curtius, J., and Carslaw, K. S.: Reduced anthropogenic aerosol
730 radiative forcing caused by biogenic new particle formation, *Proceedings of the National Academy of*
731 *Sciences of the United States of America*, 113, 12053-12058, 10.1073/pnas.1602360113, 2016.
- 732 Guo, H., Wang, D. W., Cheung, K., Ling, Z. H., Chan, C. K., and Yao, X. H.: Observation of aerosol
733 size distribution and new particle formation at a mountain site in subtropical Hong Kong, *Atmospheric*
734 *Chemistry and Physics*, 12, 9923-9939, 10.5194/acp-12-9923-2012, 2012.
- 735 Gysel, M., Crosier, J., Topping, D. O., Whitehead, J. D., Bower, K. N., Cubison, M. J., Williams, P. I.,
736 Flynn, M. J., McFiggans, G. B., and Coe, H.: Closure study between chemical composition and
737 hygroscopic growth of aerosol particles during TORCH2, *Atmos. Chem. Phys.*, 7, 6131-6144,
738 10.5194/acp-7-6131-2007, 2007.
- 739 Hallar, A. G., Lowenthal, D. H., Chirokova, G., Borys, R. D., and Wiedinmyer, C.: Persistent daily new
740 particle formation at a mountain-top location, *Atmospheric Environment*, 45, 4111-4115,
741 10.1016/j.atmosenv.2011.04.044, 2011.
- 742 Herrmann, E., Weingartner, E., Henne, S., Vuilleumier, L., Bukowiecki, N., Steinbacher, M., Conen, F.,
743 Collaud Coen, M., Hammer, E., Jurányi, Z., Baltensperger, U., and Gysel, M.: Analysis of long-term
744 aerosol size distribution data from Jungfraujoch with emphasis on free tropospheric conditions, cloud
745 influence, and air mass transport, *Journal of Geophysical Research: Atmospheres*, 120, 9459-9480,
746 10.1002/2015jd023660, 2015.



- 747 Huang, X., Zhou, L., Ding, A., Qi, X., Nie, W., Wang, M., Chi, X., Petäjä T., Kerminen, V. M., Roldin,
748 P., Rusanen, A., Kulmala, M., and Boy, M.: Comprehensive modelling study on observed new particle
749 formation at the SORPES station in Nanjing, China, *Atmos. Chem. Phys.*, 16, 2477-2492,
750 10.5194/acp-16-2477-2016, 2016.
- 751 Hussein, T., Dal Maso, M., Petaja, T., Koponen, I. K., Paatero, P., Aalto, P. P., Hameri, K., and Kulmala,
752 M.: Evaluation of an automatic algorithm for fitting the particle number size distributions, *Boreal*
753 *Environ. Res.*, 10, 337-355, 2005.
- 754 Järvinen, E., Virkkula, A., Nieminen, T., Aalto, P. P., Asmi, E., Lanconelli, C., Busetto, M., Lupi, A.,
755 Schioppo, R., Vitale, V., Mazzola, M., Petäjä T., Kerminen, V. M., and Kulmala, M.: Seasonal cycle
756 and modal structure of particle number size distribution at Dome C, Antarctica, *Atmospheric Chemistry*
757 *and Physics*, 13, 7473-7487, 10.5194/acp-13-7473-2013, 2013.
- 758 Jaeglé L., Jacob, D. J., Wang, Y., Weinheimer, A. J., Ridley, B. A., Campos, T. L., Sachse, G. W., and
759 Hagen, D. E.: Sources and chemistry of NO_x in the upper troposphere over the United States,
760 *Geophysical Research Letters*, 25, 1705-1708, 10.1029/97gl03591, 1998.
- 761 Kivekäs, N., Sun, J., Zhan, M., Kerminen, V. M., Hyvärinen, A., Komppula, M., Viisanen, Y., Hong, N.,
762 Zhang, Y., Kulmala, M., Zhang, X. C., Deli, G., and Lihavainen, H.: Long term particle size
763 distribution measurements at Mount Waliguan, a high-altitude site in inland China, *Atmos. Chem.*
764 *Phys.*, 9, 5461-5474, 10.5194/acp-9-5461-2009, 2009.
- 765 Komppula, M., Lihavainen, H., Hyvärinen, A. P., Kerminen, V. M., Panwar, T. S., Sharma, V. P., and
766 Viisanen, Y.: Physical properties of aerosol particles at a Himalayan background site in India, *Journal*
767 *of Geophysical Research*, 114, 10.1029/2008jd011007, 2009.
- 768 Kulmala, M., maso, M. D., Mäkelä J. M., Pirjola, L., Väkevä M., Aalto, P., Miiikkulainen, P., Hämeri,
769 K., #039, and dowd, C. D.: On the formation, growth and composition of nucleation mode particles,
770 2001, 53, 10.3402/tellusb.v53i4.16622, 2001.
- 771 Lüthi, Z. L., Škerlak, B., Kim, S. W., Lauer, A., Mues, A., Rupakheti, M., and Kang, S.: Atmospheric
772 brown clouds reach the Tibetan Plateau by crossing the Himalayas, *Atmos. Chem. Phys.*, 15,
773 6007-6021, 10.5194/acp-15-6007-2015, 2015.
- 774 Laing, J. R., Jaffe, D. A., and Hee, J. R.: Physical and optical properties of aged biomass burning
775 aerosol from wildfires in Siberia and the Western USA at the Mt. Bachelor Observatory, *Atmos. Chem.*
776 *Phys.*, 16, 15185-15197, 10.5194/acp-16-15185-2016, 2016.
- 777 Latham, T. L., Beyersdorf, A. J., Thornhill, K. L., Winstead, E. L., Cubison, M. J., Hecobian, A.,
778 Jimenez, J. L., Weber, R. J., Anderson, B. E., and Nenes, A.: Analysis of CCN activity of Arctic aerosol
779 and Canadian biomass burning during summer 2008, *Atmospheric Chemistry and Physics*, 13,
780 2735-2756, 10.5194/acp-13-2735-2013, 2013.
- 781 Lunden, M. M., Black, D. R., McKay, M., Revzan, K. L., Goldstein, A. H., and Brown, N. J.:
782 Characteristics of Fine Particle Growth Events Observed Above a Forested Ecosystem in the Sierra
783 Nevada Mountains of California, *Aerosol Science and Technology*, 40, 373-388,
784 10.1080/02786820600631896, 2006.
- 785 Merikanto, J., Spracklen, D. V., Mann, G. W., Pickering, S. J., and Carslaw, K. S.: Impact of nucleation
786 on global CCN, *Atmospheric Chemistry And Physics*, 9, 8601-8616, 10.5194/acp-9-8601-2009, 2009.
- 787 Neitola, K., Asmi, E., Komppula, M., Hyvärinen, A. P., Raatikainen, T., Panwar, T. S., Sharma, V. P.,
788 and Lihavainen, H.: New particle formation infrequently observed in Himalayan foothills – why?,
789 *Atmospheric Chemistry and Physics*, 11, 8447-8458, 10.5194/acp-11-8447-2011, 2011.
- 790 Nishita, C., Osada, K., Kido, M., Matsunaga, K., and Iwasaka, Y.: Nucleation mode particles in upslope



- 791 valley winds at Mount Norikura, Japan: Implications for the vertical extent of new particle formation
792 events in the lower troposphere, *Journal of Geophysical Research*, 113, 10.1029/2007jd009302, 2008.
- 793 Okamoto, S., and Tanimoto, H.: A review of atmospheric chemistry observations at mountain sites,
794 *Progress in Earth and Planetary Science*, 3, 10.1186/s40645-016-0109-2, 2016.
- 795 Peng, J. F., Hu, M., Wang, Z. B., Huang, X. F., Kumar, P., Wu, Z. J., Guo, S., Yue, D. L., Shang, D. J.,
796 Zheng, Z., and He, L. Y.: Submicron aerosols at thirteen diversified sites in China: size distribution,
797 new particle formation and corresponding contribution to cloud condensation nuclei production,
798 *Atmospheric Chemistry and Physics*, 14, 10249-10265, 10.5194/acp-14-10249-2014, 2014.
- 799 Petters, M. D., and Kreidenweis, S. M.: A single parameter representation of hygroscopic growth and
800 cloud condensation nucleus activity, *Atmos. Chem. Phys.*, 7, 1961-1971, 10.5194/acp-7-1961-2007,
801 2007.
- 802 Pierce, J. R., Leaitch, W. R., Liggio, J., Westervelt, D. M., Wainwright, C. D., Abbatt, J. P. D., Ahlm, L.,
803 Al-Basheer, W., Cziczo, D. J., Hayden, K. L., Lee, A. K. Y., Li, S. M., Russell, L. M., Sjostedt, S. J.,
804 Strawbridge, K. B., Travis, M., Vlasenko, A., Wentzell, J. J. B., Wiebe, H. A., Wong, J. P. S., and
805 Macdonald, A. M.: Nucleation and condensational growth to CCN sizes during a sustained pristine
806 biogenic SOA event in a forested mountain valley, *Atmos. Chem. Phys.*, 12, 3147-3163,
807 10.5194/acp-12-3147-2012, 2012.
- 808 Rodríguez, S., González, Y., Cuevas, E., Ramos, R., Romero, P. M., Abreu-Afonso, J., and Redondas,
809 A.: Atmospheric nanoparticle observations in the low free troposphere during upward orographic flows
810 at Izaña Mountain Observatory, *Atmos. Chem. Phys.*, 9, 6319-6335, 10.5194/acp-9-6319-2009, 2009.
- 811 Rose, C., Sellegri, K., Freney, E., Dupuy, R., Colomb, A., Pichon, J. M., Ribeiro, M., Bourianne, T.,
812 Burnet, F., and Schwarzenboeck, A.: Airborne measurements of new particle formation in the free
813 troposphere above the Mediterranean Sea during the HYMEX campaign, *Atmospheric Chemistry and*
814 *Physics*, 15, 10203-10218, 10.5194/acp-15-10203-2015, 2015.
- 815 Shen, X., Sun, J., Zhang, X., Kivekää, N., Zhang, Y., Wang, T., Zhang, X., Yang, Y., Wang, D., Zhao, Y.,
816 and Qin, D.: Particle Climatology in Central East China Retrieved from Measurements in Planetary
817 Boundary Layer and in Free Troposphere at a 1500-m-High Mountaintop Site, *Aerosol and Air Quality*
818 *Research*, 16, 659-701, 10.4209/aaqr.2015.02.0070, 2016.
- 819 Shen, X. J., Sun, J. Y., Zhang, Y. M., Wehner, B., Nowak, A., Tuch, T., Zhang, X. C., Wang, T. T., Zhou,
820 H. G., Zhang, X. L., Dong, F., Birmili, W., and Wiedensohler, A.: First long-term study of particle
821 number size distributions and new particle formation events of regional aerosol in the North China
822 Plain, *Atmospheric Chemistry and Physics*, 11, 1565-1580, 10.5194/acp-11-1565-2011, 2011.
- 823 Sipilä M., Berndt, T., Petäjä T., Brus, D., Vanhanen, J., Stratmann, F., Patokoski, J., Mauldin, R. L.,
824 Hyvärinen, A.-P., Lihavainen, H., and Kulmala, M.: The Role of Sulfuric Acid in Atmospheric
825 Nucleation, *Science*, 327, 1243-1246, 10.1126/science.1180315, 2010.
- 826 Tröstl, J., Chuang, W. K., Gordon, H., Heinritzi, M., Yan, C., Molteni, U., Ahlm, L., Frege, C., Bianchi,
827 F., Wagner, R., Simon, M., Lehtipalo, K., Williamson, C., Craven, J. S., Duplissy, J., Adamov, A.,
828 Almeida, J., Bernhammer, A.-K., Breitenlechner, M., Brilke, S., Dias, A., Ehrhart, S., Flagan, R. C.,
829 Franchin, A., Fuchs, C., Guida, R., Gysel, M., Hansel, A., Hoyle, C. R., Jokinen, T., Junninen, H.,
830 Kangasluoma, J., Keskinen, H., Kim, J., Krapf, M., Kürten, A., Laaksonen, A., Lawler, M., Leiminger,
831 M., Mathot, S., Mähler, O., Nieminen, T., Onnela, A., Petäjä T., Piel, F. M., Miettinen, P., Rissanen, M.
832 P., Rondo, L., Sarnela, N., Schobesberger, S., Sengupta, K., Sipilä M., Smith, J. N., Steiner, G., Tomé
833 A., Virtanen, A., Wagner, A. C., Weingartner, E., Wimmer, D., Winkler, P. M., Ye, P., Carslaw, K. S.,
834 Curtius, J., Dommen, J., Kirkby, J., Kulmala, M., Riipinen, I., Worsnop, D. R., Donahue, N. M., and



- 835 Baltensperger, U.: The role of low-volatility organic compounds in initial particle growth in the
836 atmosphere, *Nature*, 533, 527-531, 10.1038/nature18271, 2016a.
- 837 Tröstl, J., Herrmann, E., Frege, C., Bianchi, F., Molteni, U., Bukowiecki, N., Hoyle, C. R., Steinbacher,
838 M., Weingartner, E., Dommen, J., Gysel, M., and Baltensperger, U.: Contribution of new particle
839 formation to the total aerosol concentration at the high-altitude site Jungfrauoch (3580 m asl,
840 Switzerland), *Journal of Geophysical Research: Atmospheres*, 121, 11,692-611,711,
841 10.1002/2015jd024637, 2016b.
- 842 Wang, Z., Wu, Z., Yue, D., Shang, D., Guo, S., Sun, J., Ding, A., Wang, L., Jiang, J., Guo, H., Gao, J.,
843 Cheung, H. C., Morawska, L., Keywood, M., and Hu, M.: New particle formation in China: Current
844 knowledge and further directions, *The Science of the total environment*, 577, 258-266,
845 10.1016/j.scitotenv.2016.10.177, 2017.
- 846 Wang, Z. B., Hu, M., Yue, D. L., Zheng, J., Zhang, R. Y., Wiedensohler, A., Wu, Z. J., Nieminen, T.,
847 and Boy, M.: Evaluation on the role of sulfuric acid in the mechanisms of new particle formation for
848 Beijing case, *Atmospheric Chemistry and Physics*, 11, 12663-12671, 10.5194/acp-11-12663-2011,
849 2011.
- 850 Wang, Z. B., Hu, M., Sun, J. Y., Wu, Z. J., Yue, D. L., Shen, X. J., Zhang, Y. M., Pei, X. Y., Cheng, Y. F.,
851 and Wiedensohler, A.: Characteristics of regional new particle formation in urban and regional
852 background environments in the North China Plain, *Atmospheric Chemistry and Physics*, 13,
853 12495-12506, 10.5194/acp-13-12495-2013, 2013.
- 854 Weller, R., Schmidt, K., Teinilä K., and Hillamo, R.: Natural new particle formation at the coastal
855 Antarctic site Neumayer, *Atmospheric Chemistry and Physics*, 15, 11399-11410,
856 10.5194/acp-15-11399-2015, 2015.
- 857 Wu, Z., Hu, M., Liu, S., Wehner, B., Bauer, S., Maßling, A., Wiedensohler, A., Petäjä T., Dal Maso,
858 M., and Kulmala, M.: New particle formation in Beijing, China: Statistical analysis of a 1-year data set,
859 *Journal of Geophysical Research*, 112, 10.1029/2006jd007406, 2007.
- 860 Wu, Z., Hu, M., Lin, P., Liu, S., Wehner, B., and Wiedensohler, A.: Particle number size distribution in
861 the urban atmosphere of Beijing, China, *Atmospheric Environment*, 42, 7967-7980,
862 10.1016/j.atmosenv.2008.06.022, 2008.
- 863 Wu, Z. J., Poulain, L., Henning, S., Dieckmann, K., Birmili, W., Merkel, M., van Pinxteren, D.,
864 Spindler, G., Müller, K., Stratmann, F., Herrmann, H., and Wiedensohler, A.: Relating particle
865 hygroscopicity and CCN activity to chemical composition during the HCCT-2010 field campaign,
866 *Atmos. Chem. Phys.*, 13, 7983-7996, 10.5194/acp-13-7983-2013, 2013.
- 867 Wu, Z. J., Zheng, J., Shang, D. J., Du, Z. F., Wu, Y. S., Zeng, L. M., Wiedensohler, A., and Hu, M.:
868 Particle hygroscopicity and its link to chemical composition in the urban atmosphere of Beijing, China,
869 during summertime, *Atmos. Chem. Phys.*, 16, 1123-1138, 10.5194/acp-16-1123-2016, 2016.
- 870 Xu, J., Wang, Z., Yu, G., Qin, X., Ren, J., and Qin, D.: Characteristics of water soluble ionic species in
871 fine particles from a high altitude site on the northern boundary of Tibetan Plateau: Mixture of mineral
872 dust and anthropogenic aerosol, *Atmospheric Research*, 143, 43-56, 10.1016/j.atmosres.2014.01.018,
873 2014.
- 874 Xu, J. Z., Zhang, Q., Wang, Z. B., Yu, G. M., Ge, X. L., and Qin, X.: Chemical composition and size
875 distribution of summertime PM_{2.5} at a high altitude remote location in the northeast of the Qinghai-
876 Xizang (Tibet) Plateau: insights into aerosol sources and processing in free troposphere, *Atmospheric
877 Chemistry and Physics*, 15, 5069-5081, 10.5194/acp-15-5069-2015, 2015.
- 878 Yli-Juuti, T., Riipinen, I., Aalto, P. P., Nieminen, T., Maenhaut, W., Janssens, I. A., Claeys, M., Salma,



879 I., Ocskay, R., Hoffer, A., Imre, K., and Kulmala, M.: Characteristics of new particle formation events
880 and cluster ions at K-pusztá, Hungary, *Boreal Environ. Res.*, 14, 683-698, 2009.

881 Yu, F., and Hallar, A. G.: Difference in particle formation at a mountaintop location during spring and
882 summer: Implications for the role of sulfuric acid and organics in nucleation, *Journal of Geophysical*
883 *Research: Atmospheres*, 119, 12,246-212,255, 10.1002/2014jd022136, 2014.

884 Yue, D. L., Hu, M., Zhang, R. Y., Wang, Z. B., Zheng, J., Wu, Z. J., Wiedensohler, A., He, L. Y., Huang,
885 X. F., and Zhu, T.: The roles of sulfuric acid in new particle formation and growth in the mega-city of
886 Beijing, *Atmospheric Chemistry And Physics*, 10, 4953-4960, 10.5194/acp-10-4953-2010, 2010.

887 Zellweger, C., Forrer, J., Hofer, P., Nyeki, S., Schwarzenbach, B., Weingartner, E., Ammann, M., and
888 Baltensperger, U.: Partitioning of reactive nitrogen (NO_y) and dependence on meteorological
889 conditions in the lower free troposphere, *Atmos. Chem. Phys.*, 3, 779-796, 10.5194/acp-3-779-2003,
890 2003.

891 Zhang, R., Khalizov, A., Wang, L., Hu, M., and Xu, W.: Nucleation and growth of nanoparticles in the
892 atmosphere, *Chemical reviews*, 112, 1957-2011, 10.1021/cr2001756, 2012.

893 Zhang, X., Yin, Y., Lin, Z., Han, Y., Hao, J., Yuan, L., Chen, K., Chen, J., Kong, S., Shan, Y., Xiao, H.,
894 and Tan, W.: Observation of aerosol number size distribution and new particle formation at a
895 mountainous site in Southeast China, *The Science of the total environment*, 575, 309-320,
896 10.1016/j.scitotenv.2016.09.212, 2016.

897 Zheng, J., Hu, M., Peng, J., Wu, Z., Kumar, P., Li, M., Wang, Y., and Guo, S.: Spatial distributions and
898 chemical properties of PM_{2.5} based on 21 field campaigns at 17 sites in China, *Chemosphere*, 159,
899 480-487, 10.1016/j.chemosphere.2016.06.032, 2016.

900 Zheng, J., Hu, M., Du, Z., Shang, D., Gong, Z., Qin, Y., Fang, J., Gu, F., Li, M., Peng, J., Li, J., Zhang,
901 Y., Huang, X., He, L., Wu, Y., and Guo, S.: Influence of biomass burning from South Asia at a
902 high-altitude mountain receptor site in China, *Atmos. Chem. Phys.*, 17, 6853-6864,
903 10.5194/acp-17-6853-2017, 2017.

904